# Molecular and Crystal Structures of Inulin from Electron Diffraction Data

**I. André,[†] K. Mazeau,[†] I. Tvaroska,[†,‡] J.-L. Putaux,[†] W. T. Winter,[§] F. R. Taravel,[†] and H. Chanzy*[,†]**

*Centre de Recherches sur les Macromolécules Végétales, CNRS, Affiliated with the Joseph Fourier University of Grenoble, B.P. 53, 38041 Grenoble Cedex 9, France, Institute of Chemistry, Slovak Academy of Sciences, SK-84238 Bratislava, Slovak Republic, and College of Environmental Science and Forestry, State University of New York, Syracuse, New York 13210*

*Received December 5, 1995; Revised Manuscript Received April 8, 1996*[⊗]

ABSTRACT: The crystal and molecular structures of inulin, the poly(2→1)-$\beta$-D-fructofuranan, hemihydrate and monohydrate, were determined by a constrained linked-atom least-squares (LALS) refinement, utilizing intensities measured from electron diffraction data and stereochemical restraints. Single crystals were grown from dilute aqueous ethanol solutions and their three-dimensional electron diffraction diagrams analyzed. In the hemihydrate form, there is half a molecule of water per fructosyl residue. In this allomorph, which corresponds to air-dried crystals, inulin adopts an orthorhombic $P2_12_12_1$ space group with cell parameters $a = 16.70$ Å, $b = 9.65$ Å, and $c$ (chain axis) $= 14.4$ Å. By using the base plane electron diffraction data combined with the upper layer line data, the best molecular model was refined to an $R$ factor of 22.7% and $R''$ factor of 22.3%. This model has two antiparallel sixfold helices centered on the twofold screw axes intersecting the base plane of the orthorhombic system. The six water molecules are distributed over eight sites in the unit cell. The helical conformation is characterized by $\phi = 66°$, $\psi = 154°$, and $\omega = -82°$. In the monohydrate form obtained when inulin crystals were kept in a moist environment, there is one molecule of water per fructosyl residue. The unit cell dimensions remained nearly the same ($a = 16.70$ Å, $b = 9.80$ Å, and $c$ (chain axis) $= 14.7$ Å) but substantial differences in the electron diffraction intensities were observed. The best molecular model was refined to an $R$ factor of 18.1% and an $R''$ factor of 16.5% by using only $hk0$ reflections of the base plane electron diffraction data. Simulated diffraction patterns of this structure showed that its differences with the hemihydrate could be accounted for only by introducing extra water molecules into the gaps of the crystalline structure without major modification of the inulin conformation.

## Introduction

This paper deals with the crystal and molecular structure of inulin, the poly (2→1)-$\beta$-D-fructofuranan. This polysaccharide, which occurs as a food reserve in a number of plants,[1] is known to crystallize readily from aqueous solution[2] but not from anhydrous mediums.[3] Normally, the molecular weight of inulin is too low to be amenable to an X-ray fiber study. This is why only X-ray powder patterns, containing up to nine diffraction rings in the best cases, have been recorded so far. The paucity of these data is insufficient to resolve the structure of crystalline inulin. In 1980, Marchessault *et al.* showed that inulin could be crystallized easily in the form of single crystals.[4] These authors, however, could not record more than three independent electron-diffraction intensity data. Even in combination with their electron diffraction, the X-ray powder diagram data were not sufficient to determine completely the inulin structure.

In a previous paper,[5] we described how more perfectly ordered single crystals of inulin could be grown from inulin fractions with narrow molecular weight distribution. These crystals gave fairly well-resolved three-dimensional electron diffraction diagrams indicating that there were two inulin polymorphs, namely a semihydrate and a hydrate that depended on the conditions of hydration of the crystals. In the present paper, the electron diffraction intensity data obtained from each of these polymorphs have been used to determine its most probable three-dimensional crystal and molecular structures.

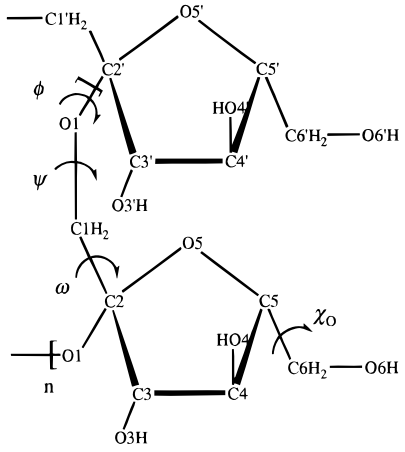


**Figure 1.** Representation of the atomic labeling scheme for the inulin chain.

## Experimental Section

**Nomenclature.** The recommendations and symbols proposed by the Commission on Nomenclature[6] have been used throughout this paper. A representation of the atomic labeling scheme is shown in Figure 1. The relative orientation of two contiguous residues is described by two bond angles $\tau_1 = C2'-O1-C1$ and $\tau_2 = O1-C1-C2$ and a set of three torsion angles: $\phi = C1'-C2'-O1-C1$, $\psi = C2'-O1-C1-C2$, and $\omega = O1-C1-C2-O5$. As usual, the orientation of the hydroxymethyl group is described by two letters, the first one referring

* To whom correspondence should be addressed.
[†] Centre de Recherches sur les Macromolécules Végétales, CNRS.
[‡] Institute of Chemistry, Slovak Academy of Sciences.
[§] College of Environmental Science and Forestry, State University of New York.
[⊗] Abstract published in *Advance ACS Abstracts,* May 15, 1996.

S0024-9297(95)01799-2 CCC: $12.00 

to the torsion angle $\chi_o$ (O5−C5−C6−O6) and the second one to the torsion angle $\chi_c$ (C4−C5−C6−O6). In this terminology, there are three possible low-energy conformations, i.e., gauche−trans (*gt*), gauche−gauche (*gg*), or trans−gauche (*tg*).[7]

**Electron Microscopy and Electron Diffraction Analysis.** Single crystals of inulin were prepared following the procedure described previously.[5] When kept in their mother liquor, the hydrated crystals contained a number of intracrystalline water molecules. Upon air-drying, part of the crystallization water left the crystals to yield a semihydrated crystalline structure.

For electron diffraction studies, drops of crystal suspensions were allowed to dry on carbon-coated grids. The semihydrated crystals resulted from air-drying, while the hydrated state required equilibration of the crystals for 48 h in a 95% relative humidity environment. The semihydrated crystals were observed under standard low-dose electron microscopy conditions. For the hydrated crystals, a low-temperature specimen holder was used, and the samples were observed with the quench-freezing technique.[8]

All electron diffraction patterns were recorded under low-dose conditions on Agfa Scientia films using a Philips CM 200 CRYO transmission electron microscope operated at 200 kV and equipped with a Lhesa image intensifier. For the semihydrated crystals, the *hk*0 reflections were collected from lamellar crystals with the lamellar plane aligned perpendicular to the electron beam, while (*hkl*) reflections were collected by rotation of the crystals about *a** by ±18°, ±24°, ±34°, and ±53° corresponding to the [01$\bar{2}$], [02$\bar{3}$], [01$\bar{1}$], and [02$\bar{1}$] zones, respectively. Similarly, rotation of the crystals about *b** by ±21°, ±25°, ±30°, ±38°, and ±49° allowed the collection of the reflections corresponding to the [10$\bar{3}$], [20$\bar{5}$], [10$\bar{2}$], [20$\bar{3}$], and [10$\bar{1}$] zones.

For the hydrated crystals that were observed with the low-dose temperature holder, instrumental limitations prevent aligning the crystals with respect to the tilt axis of the microscope. Only those crystals having either their *a** or *b** axis parallel to the tilt axis of the electron microscope were considered. These crystals were rotated by the same angles as those of the semihydrated crystals.

The intensities of both *hk*0 and *hkl* reflections were measured by scanning the diffractograms with a Joyce-Loebl recording microdensitometer calibrated with a stepped precision gray scale. Special care was taken to record diffraction patterns with a range of exposure times in order to ensure that the intensities of the spots of interest did not saturate the photographic emulsion. All the *hk*0 diffractograms were scaled with respect to one another by summing all the observed intensities in each diagram and scaling these sums. After scaling, the intensity of each reflection taken from the series of diagrams was averaged and individual *F*(*hk*0) were taken as the square root of the corresponding intensities. In the *hkl* diagrams, those spots with *hk*0 indices were employed as standards to scale these patterns with respect to the *hk*0 diffractograms. *F*(*hkl*) were taken as the square root of the corresponding intensities.

For the semihydrated allomorph, the *hk*0 data set included 10 measurable independent reflections, 5 systematic absences for odd orders of *h*00 and 0*k*0, and 13 reflections below the observational threshold. The *hkl* data set contained an additional 16 observable reflections together with 9 below the observational threshold. Within each diagram, the unobserved reflections within the sphere of diffraction were assigned relative intensities of one-third of the minimum observable value in the corresponding diffractogram. Similarly for the inulin hydrate, the *hk*0 data set included 22 observed independent reflections out of which only 14 were strong enough to be measured. The other eight were visible but too weak to be measured. A visual estimate of their intensities gave a value intermediate between the unobserved threshold and the weakest measurable observed value. There were also 5 systematic absences for odd orders of *h*00 and 0*k*0 and 10 reflections below the observable threshold. As for the semihydrate crystals, these unobserved reflections were also assigned a relative intensity of one-third of the minimum observable value in the corresponding diffractogram.

**X-ray Diffraction.** Aqueous suspensions of inulin crystals were allowed to dry in flat-bottom polyethylene capsules. X-ray diffraction data from the resulting films were obtained with the incident X-ray beam either parallel or perpendicular to the plane of the sample. A Wahrus flat-film X-ray vacuum camera mounted on a Philips 1720 X-ray generator operated with Ni-filtered Cu Kα radiation ($\lambda = 1.5418$ Å) was used for the experiments. The films of semihydrated crystals were analyzed under vacuum whereas those of hydrated crystals were X-rayed in thin-walled glass capillaries. Prior to sealing, these capillaries were equilibrated for 48 h in 95% relative humidity environment at room temperature.

**Structure Refinement.** The initial coordinates of the fructofuranose ring were taken from the study of Calub *et al.* on the conformational analysis of inulobiose.[9] Possible sixfold helical single-chain models were generated and used as starting models. For this purpose, the helical parameters *n* (the number of residues per turn) and *h* (the projected height of the residue onto the helix axis) were calculated with the HELIPOL program[10] for each ($\phi$, $\psi$) pair (by stepping these angles at 10° intervals) and for the three positions of $\omega$, namely 60°, −60°, and 180°.

A version of the linked-atom least-squares (LALS) refinement program[11] modified for the use of electron diffraction data[12] was used throughout the refinement of the structure. The form factors for electron diffraction for atomic species C, O, and H were taken from the International Tables of X-ray Crystallography.[13] Contact parameters used in the stereochemical refinement are those of Arnott and Winter.[14] The residuals *R* and *R*″ are defined in ref 15. These values were calculated using *B* (isotropic temperature factors) of 4.0 for all atoms, including those of the water molecules.

Simulations of the X-ray and electron diffraction patterns of the structures obtained for the two inulin polymorphs were carried out using the CERIUS[16] software running on Silicon Graphics Indigo workstation. All other calculations were carried out on a Sun Sparc 2 workstation. Molecular drawings were performed using QUANTA[16] software.

## Results

In a previous study,[5] it was shown that inulin could be crystallized as either of two crystalline polymorphs, namely a semihydrated and a hydrated form. In the semihydrated form, inulin crystallizes in space group $P2_12_12_1$ with unit cell dimensions $a = 16.70$ Å, $b = 9.65$ Å, and $c$ (chain axis) $= 14.4$ Å. Thus, in conjunction with density measurements, it was shown that the unit cell contained two antiparallel sixfold helices, each centered on a crystallographic twofold screw axis parallel to *c*. In addition, this structure contains six water molecules, i.e. one molecule of water per two fructosyl residues. Hence, the semihydrated inulin structure is in fact a hemihydrate. Upon further hydration, the unit cell of the hemihydrate became slightly swollen with new cell parameters $a = 16.70$ Å, $b = 9.80$ Å, and $c = 14.7$ Å while keeping the $P2_12_12_1$ symmetry. The main difference between the hemihydrate and this hydrated inulin was in the number of water molecules in the unit cell. As a reproducible value of the density of the hydrated crystals could not be obtained, it was difficult to define accurately the increase in water content resulting from the hydration phenomenon. However, the maximum number of water molecules that could be accommodated by molecular modeling in this structure was 12, i.e. one molecule of water per fructosyl residue. Thus, the hydrated structure of inulin can be described as a monohydrate.

**Inulin Hemihydrate.** Theoretical studies[17] on the flexibility of the fructofuranose ring indicate that the dominant conformation of the fructofuranose ring in mono- and oligosaccharides is the $^4T_3$ form. Hence, this conformation was selected for the present study. The

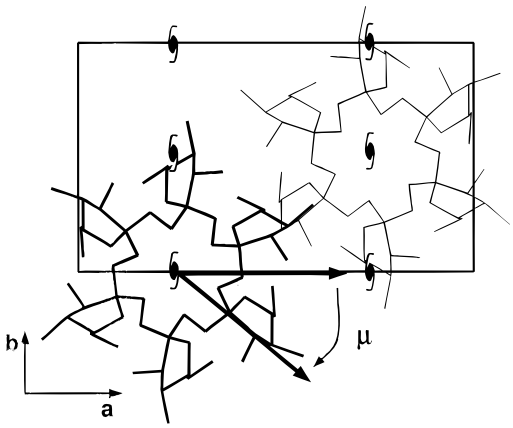


**Figure 2.** Representation of the $\mu$ angle defining the orientation of the polymer chain with respect to the unit cell edge *a*.

linkage geometry—bond lengths, bond angles, and torsion angles, taken from the inulobiose model[9]—were used to construct the initial inulin chain. The helical parameters *n* and *h* calculated as described in the Experimental Section were plotted as iso-*n* and iso-*h* contours on the three maps corresponding to the three $\omega$ positions. From these maps, several values of the torsion angles $\phi$, $\psi$, and $\omega$ consistent with symmetry constraints imposed by the *c* dimension of the unit cell and the sixfold symmetry were found at the intersection of the corresponding iso-*n* ($n = 6$) and iso-*h* ($h = 2.4$ Å) contours. The restrictions imposed by these criteria led to 31 possible starting single-chain conformations distributed between right- and left-handed models. Each of these different models was minimized with the LALS program. The refinement was carried out in several steps. First, for each model, a refinement of the molecular structure against the nonbonded interaction energy was performed by optimizing the $\phi$, $\psi$, and $\omega$ torsion angles to build an exact sixfold helix fitting into the $c = 14.4$ Å repeat. The choice of the exact sixfold helix is not governed by symmetry consideration but was used here for simplification. The position of the chain helix axis was then set in coincidence with one of the $2_1$ crystallographic axes parallel to the *c* parameter of the unit cell. This positioning was the only possibility that could combine at the same time the choice of the $P2_12_12_1$ space group with the occurrence of only two chains in the unit cell. The second chain of the structure was then deduced by applying the $P2_12_12_1$ symmetry operator $(-x, {}^1/_2 + y, {}^1/_2 - z)$.

In this preliminary refinement, the 31 starting models converged toward 5 different conformers corresponding to 3 right-handed and 2 left-handed helices. For each of these models, a further refinement of the orientation of the two antiparallel chains with respect to the unit cell edge, *a*, was done systematically by stepping a variable parameter $\mu$ in 5° increments. This parameter corresponds to the angle between a vector from the helix center and parallel to the *a* edge of the unit cell and a second vector linking the helix center to carbon atom C3 defined as the root atom of inulin (Figure 2). For this optimization, only the *hk*0 data were used and the crystallographic residuals[15] *R* and *R″* were computed at each point. Of the five optimized starting models, only one model, a right-handed helix, gave a reasonable compromise between the imposed helix geometry and a good agreement with the observed structure factors. The conformation of the chain in this model is characterized by the torsion angles $\phi = 66°$, $\psi = 155°$, and $\omega = -82°$.

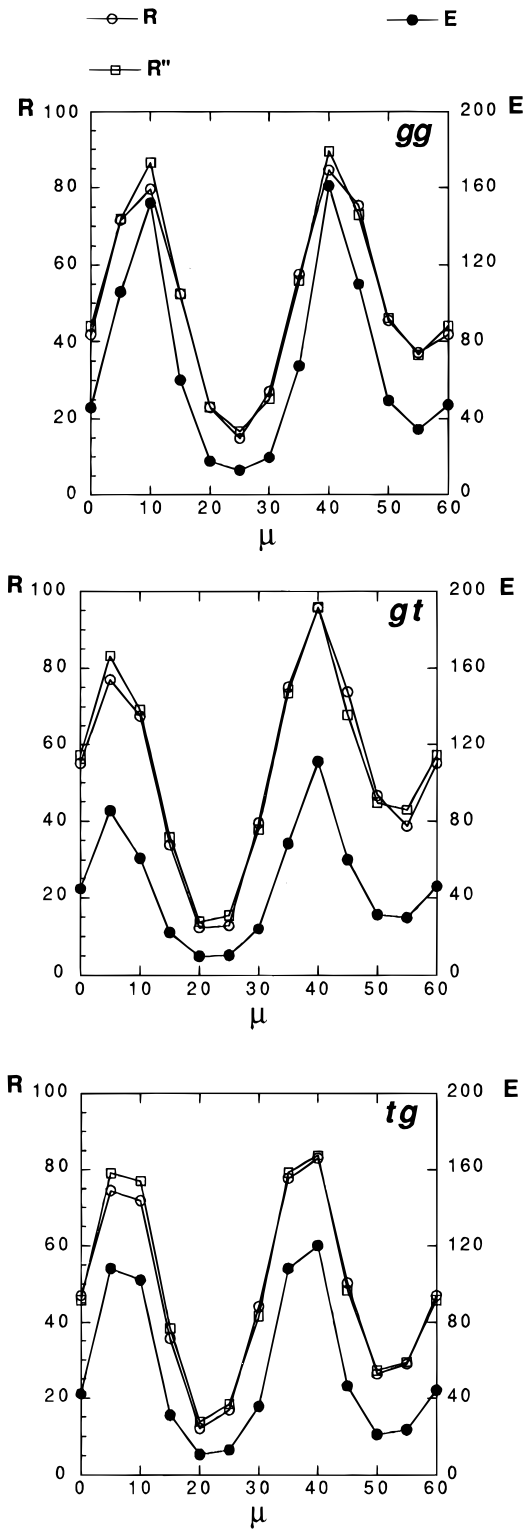


**Figure 3.** Reliability factors $R_{hk0}$ and $R''_{hk0}$ together with nonbonded interaction energy *E* as a function of the orientation angle $\mu$ for the three conformations of the hydroxymethyl group: *gg* (top), *gt* (middle), and *tg* (bottom).

In the next step, the influence of the hydroxymethyl orientation around the C5−C6 bond of the inulin structure was investigated. Using the model described above, three models, each with a different orientation of the hydroxymethyl group, corresponding to the *gg*, *gt*, or *tg* rotamer, were generated. For these models, the calculated dependencies of the nonbonded interaction energy, *E*, and the crystallographic residual, *R*, obtained from the *hk*0 diffraction data as a function of $\mu$ are shown in Figure 3. The curves look very similar.

**Table 1. Crystallographic Residuals $R_{hk0}$ and $R''_{hk0}$, $R_{hkl}$ and $R''_{hkl}$ (%), Nonbonded Interaction Energies $E$ and $E'$ (in Arbitrary Units), Chain Orientation Angle $\mu$ (deg), and Chain Translation $W$ along the $c$ Axis for the Three Inulin Hemihydrate Models Having Different Hydroxymethyl Conformations**

| | *gt* | *tg* | *gg* |
|---|---|---|---|
| $R_{hk0}$[a] | 8.9 | 11.8 | 14.4 |
| $R''_{hk0}$[a] | 12.2 | 14.1 | 15.1 |
| $E$ | 9.3 | 10.7 | 11.9 |
| $\mu$ | 20.9 | 21.6 | 27.6 |
| $R_{hkl}$[b] | 17.4 | 19.1 | 24.6 |
| $R''_{hkl}$[b] | 17.3 | 19.3 | 25.8 |
| $E'$ | 13.7 | 17.9 | 30.4 |
| $W$ | 0.7060 | 0.7042 | 0.7073 |

[a] Based on 10 observed, 13 unobserved, and 5 systematically absent reflections. [b] Based on 26 observed, 22 unobserved, and 5 systematically absent reflections.

For all three models with different values of the torsion angle $\chi_o$, two minima are found. The lowest energy minimum occurs between $\mu = 20°$ and $\mu = 30°$. The value of the $R$ factor is also the lowest at this position. A second minimum at $\mu = 55°$ is also present and was considered. Models with either of these two orientations of the inulin chain were used for further refinements by introducing the rotation of the hydroxymethyl conformation from its initial *gt*, *gg*, or *tg* position. These optimizations showed that refinements which started from an orientation angle $\mu = 20°$ led to lower reliability factors than those starting from $\mu = 55°$. For this reason, only the $\mu$ angle of 20° was considered in further study. The results obtained after refinement of the three models are shown in Table 1. The *gt* conformation refinement led to $R = 8.9\%$ and $R'' = 12.2\%$. For the other two models, the corresponding factors were higher. For the *tg* model, $R = 11.8\%$ and $R'' = 14.1\%$, and for the *gg* model, $R = 14.4\%$ and $R" = 15.1\%$ were obtained. A comparison of the values given in Table 1 suggests that a chain with the hydroxymethyl group in *gt* is the most probable model of the inulin chain. For this model, refinement gave $\mu = 20.9°$ and an energy of 9.3 in arbitrary units.

In the final step, each of the *gt*, *tg*, and *gg* models, characterized by the values given in Table 1, was further optimized by systematic translation of the parent chain along the $c$ axis and in $c/20$ steps using the full three-dimensional diffraction data. The translation was controlled by the parameter $W$, which corresponds to the fractional displacement of the root atom C3 in the unit cell parallel to the $c$ axis. The results are shown in Figure 4. This was followed by a full refinement in which all the conformational and packing parameters were optimized. The final structural parameters for the three models are summarized in Table 1. It was found that for all three models only one minimum occurred on the curves at $W = 0.7$. Considering all criteria (interaction energy, contacts, and $R$ factors), it again appears that the *gt* model is the best one. For this model, $R = 17.4\%$, $R'' = 17.3\%$, and an energy $E' = 13.7$ in arbitrary units were obtained. The other models, *tg* and *gg*, had higher energies and larger $R$ factors: $R$ and $R''$ of 19.1% and 19.3%, respectively, for the *tg* model and 24.6% and 25.8% for the *gg* one. However, it may be noticed that the difference in $R$ factors between models with *gt* and *tg* orientations around the C5−C6 bond is not very large.

The presence of six water molecules in the unit cell of the hemihydrate structure has been detected experimentally.[5] Therefore, two independent water molecules

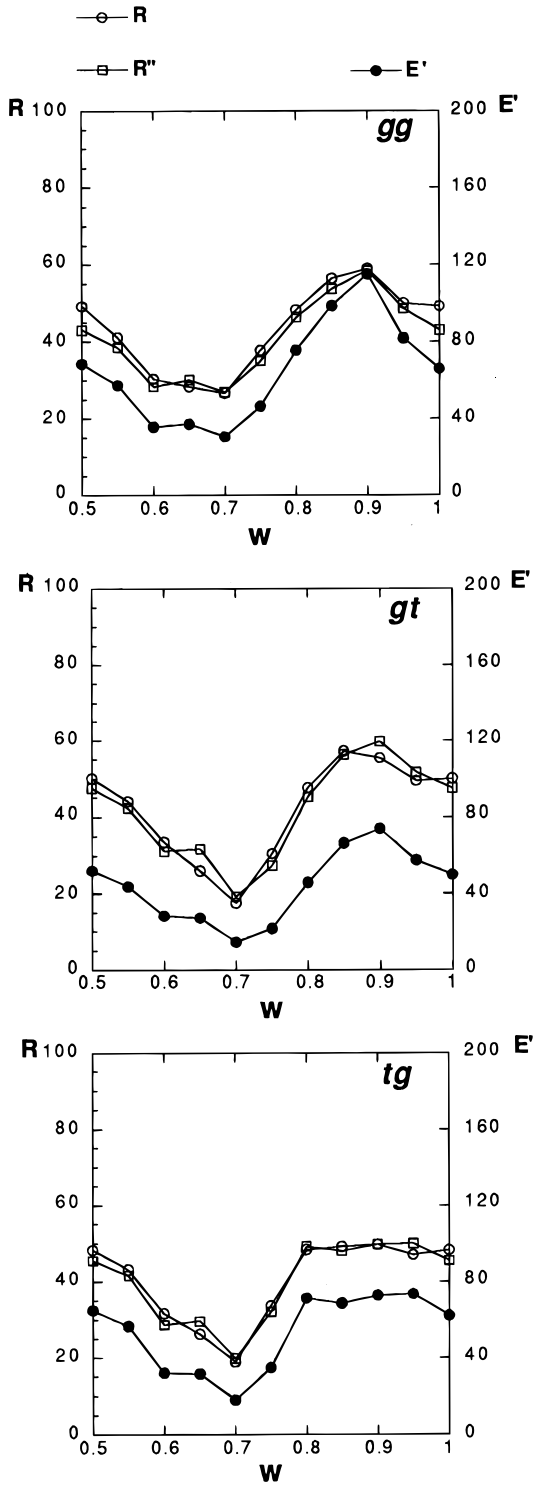


**Figure 4.** Reliability factors $R_{hkl}$ and $R''_{hkl}$ together with nonbonded interaction energy $E'$ as a function of the translation $W$ for the three conformations of the hydroxymethyl group: *gg* (top), *gt* (middle), and *tg* (bottom).

were introduced in the unit cell of the *gt* model with an occupancy of 0.75 for each one. The $P2_12_12_1$ symmetry, implies eight water molecules in the unit cell while the occupancy of 0.75 reduces the number to six. The position of these crystallographic water molecules was refined using the LALS program, starting from several trial positions and without changing either the conformation or the arrangement of the inulin chains. For this hemihydrate *gt* model, $R = 22.7\%$ and $R'' = 22.3\%$ were obtained for the complete *hkl* data set.

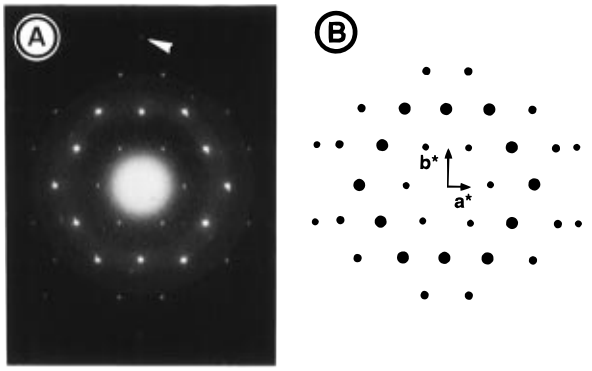


**Figure 5.** Comparison of the observed (A) and simulated (B) electron diffraction patterns for the base plane (*hk*0) of inulin hemihydrate. The arrow points toward the 040 reflection that is weak in the observed diffractogram but absent in the simulated pattern.

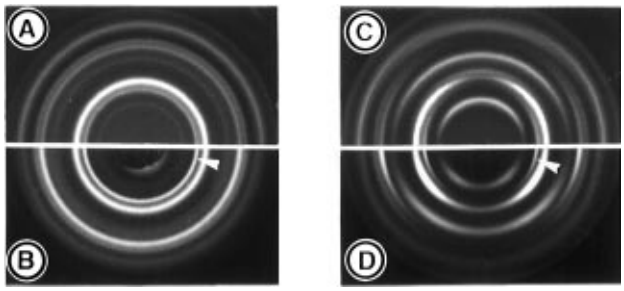


**Figure 6.** Comparison of the simulated (A and C) and observed (B and D) X-ray patterns of inulin hemihydrate. A and B correspond to powder patterns whereas C and D correspond to oriented patterns taken on crystal mats with the X-ray beam parallel to the mat surface. The arrows in B and D correspond to composite reflections 110 and 200 that are observed in inulin hemihydrate but are totally absent in inulin monohydrate.

**Table 3. Summary of Conformational Parameters and Their Final Values for the Inulin Hemihydrate *gt* Model**

| parameter | final value | parameter | final value |
|---|---|---|---|
| $\phi$ (deg) | 66.0 | $\tau_1$ (deg)[a] | 115.9 |
| $\psi$ (deg) | 154.5 | $\tau_2$ (deg)[a] | 109.2 |
| $\omega$ (deg) | −81.8 | $\mu$ (deg) | 20.98 |
| $\chi_o$ (deg) | 54.1 | W | 0.706 |
| $\chi_c$ (deg) | 176.2 | | |

[a] Unlike the other conformational parameters, $\tau_1$ and $\tau_2$ were not varied during the refinement.

The agreement between the calculated and observed structure factor amplitudes is satisfactory (Table 2 in Supporting Information). This agreement is also illustrated in Figure 5, where the observed and simulated electron diffraction patterns for the base plane (*hk*0) are compared. A similar comparison of the simulated and the experimental powder and oriented X-ray diagrams is presented in Figure 6.

A summary of the conformational parameters for the hemihydrate *gt* model is given in Table 3. The atomic coordinates are given in Table 4 (Supporting Information) whereas the hydrogen-bonding pattern is presented in Table 5. The proposed crystal model of inulin is shown in Figure 7 in the *ab* projection. In this figure, the water molecules have been omitted for clarity. Stereoviews of the structure as well as the intermolecular hydrogen bonds are presented in Figure 8.

**Inulin Monohydrate.** A determination of the structural differences between the hemihydrate and monohydrate inulin was also carried out. In a previous paper,[5] it was shown that the unit cell dimensions of both polymorphs were very similar. However, some significant differences in the intensities of the electron and X-ray diffractograms are apparent. In particular, an X-ray diffraction maximum at $d = 8.35$ Å which was present in the hemihydrate was totally absent in the monohydrate. Also, the 040 electron diffraction maximum which is absent in the monohydrate was present in the hemihydrate crystals. After unsuccessful attempts to determine experimentally the number of water molecules in the unit cell of the monohydrate structure, this determination was undertaken by molecular modeling. It was found that a total of three independent water molecules could fill the spaces between the chains. Considering the $P2_12_12_1$ space group, 12 water molecules can therefore be accommodated in the unit cell. In order to explain the differences in the diffraction patterns due to the presence of water in the structure, we began with the three models corresponding to each hydroxymethyl group conformation refined in the hemihydrate structure. Then, the unit cell dimensions were changed to the experimental values observed for the hydrated form, $a = 16.70$ Å, $b = 9.80$ Å, and $c = 14.7$ Å, and the monohydrate *hk*0 data introduced. Three independent water molecules with an occupancy factor of 1 were also introduced, in succession, into the unit cell. The conformation of the chains and the position of the three

**Table 5. Summary of Intermolecular Hydrogen Bond Interactions Stabilizing the Structure of Inulin Hemihydrate**

| donor atom | acceptor atom | *d* (Å) | residue[a] |
|---|---|---|---|
| O4 | O4 | 2.74 | $I_2-II_1$ |
| O3 | O3 | 3.34 | $I_2-II_1$ |
| O6 | O6 | 3.20 | $I_1-II_6$ |
| O3 | H4 | 2.13 | $I_2-II_1$ |
| O6 | O4 | 3.34 | $I_1-III_5$ |
| O6 | O3 | 2.86 | $I_2-III_5$ |
| O3 | O3 | 2.52 | $II_1-III_6$ |
| $O_W$ | O6 | 3.01 | $W_2(I)-I_2$ |
| $O_W$ | O4 | 2.77 | $W_4(II)-I_1$ |
| $O_W$ | O6 | 2.73 | $W_3(I)-I_1$ |
| $O_W$ | O5 | 2.67 | $W_3(I)-I_6$ |
| $O_W$ | O6 | 2.82 | $W_3(I)-I_6$ |
| $O_W$ | O4 | 3.26 | $W_3(I)-III_5$ |

[a] The chain II is defined as in Table 4. The chain III is generated from chain I by $(x', y', z') = (x, 1 + y, z)$. The atomic coordinates of the residues and those of the oxygens of the water molecules are defined as in Table 4 in the Supporting Information.

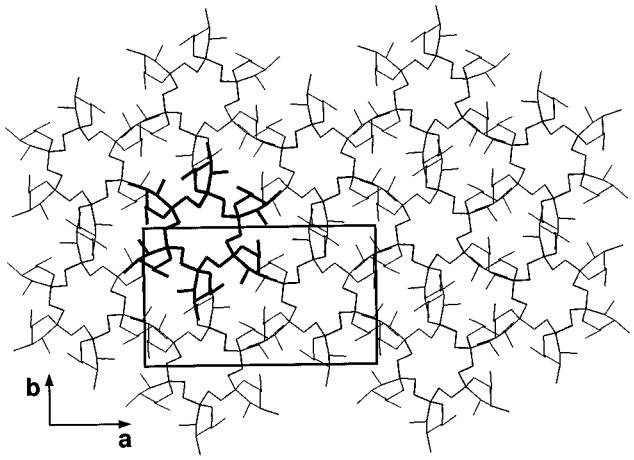


**Figure 7.** Structure of the inulin hemihydrate viewed as a projection of the unit cell onto the *ab* plane (the water molecules are not shown in order to clarify the figure).

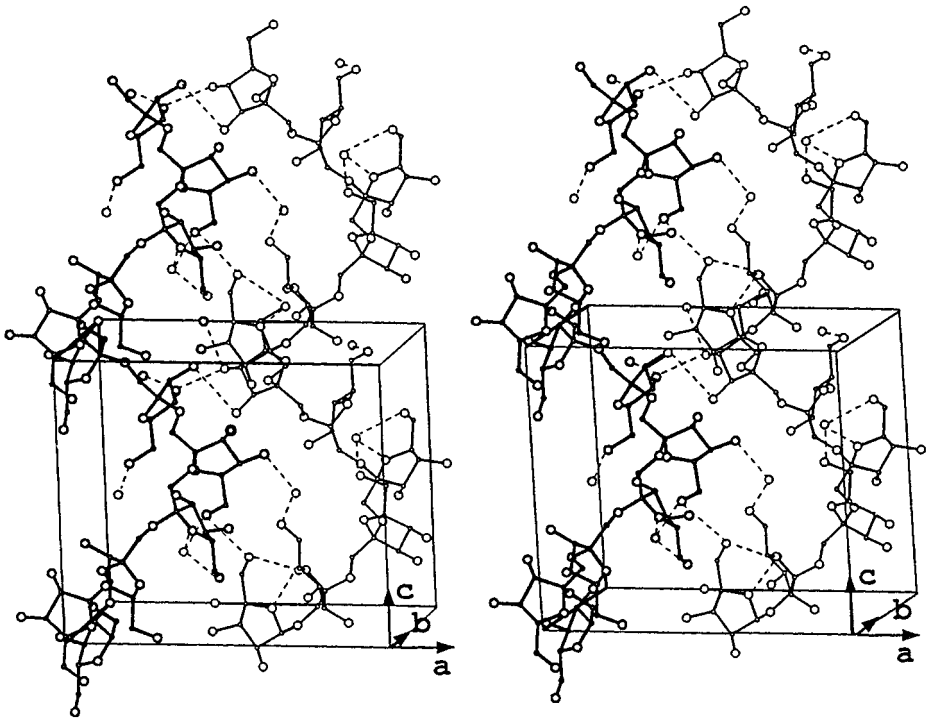


**Figure 8.** Stereoviews of the inulin hemihydrate model. The dotted lines correspond to the intermolecular hydrogen bonds.

**Table 6. Crystallographic Residuals $R_{hk0}$ and $R''_{hk0}$ (%), Nonbonded Interaction Energy $E''$ (in Arbitrary Units), Chain Orientation Angle $\mu$ (deg), and Chain Translation $W$ along the $c$ Axis for the Three Inulin Monohydrate Models with Different Hydroxymethyl Conformations**

| | *gt* | *tg* | *gg* |
|---|---|---|---|
| $R_{hk0}$[a] | 18.1 | 21.1 | 18.5 |
| $R''_{hk0}$[a] | 16.5 | 20.6 | 19.1 |
| $E''$ | 45.0 | 57.0 | 56.0 |
| $\mu$ | 21.5 | 20.4 | 24.3 |
| $W$ | 0.7150 | 0.7106 | 0.7115 |

[a] Based on 14 observed, 8 too weak to be measured, 10 unobserved, and 5 systematically absent reflections.

water molecules starting from several initial positions were then refined by optimizing the $\phi$, $\psi$, $\omega$, and $\chi_o$ torsion angles as well as the fractional coordinates of the water molecules and the rotation and the translation of the inulin chains against the nonbonded interaction energy and the $hk0$ diffraction data. It was not possible to collect scalable sets of $hkl$ intensities from the hydrated specimen. This is a consequence of the fact that a rotation, low-temperature specimen holder was not available for our transmission electron microscope. For this reason, $hkl$ intensities were not used for the refinement. The values of the crystallographic residuals $R$ and $R''$ for the three conformations *gt*, *tg*, and *gg* are listed in Table 6. A comparison of these values suggests that the *gt* hydroxymethyl conformer is again the most probable model as it yields crystallographic residuals of $R = 18.1\%$ and $R'' = 16.5\%$. The agreement between the calculated and observed structure factor amplitudes is satisfactory (Table 7 in Supporting Information). This agreement is also illustrated in Figure 9, where the observed and simulated electron diffraction patterns for the base plane ($hk0$) are compared. A similar comparison of the simulated and the experimental powder X-ray diagram is presented in Figure 10.

A summary of the conformational parameters for the hydrated *gt* model is given in Table 8. The atomic coordinates are given in Table 9 (Supporting Information) whereas the hydrogen-bonding pattern is presented in Table 10. The inulin crystal model proposed for the hydrated form is shown in Figure 11 in a pair of stereoviews which show also the intermolecular hydrogen bonds.

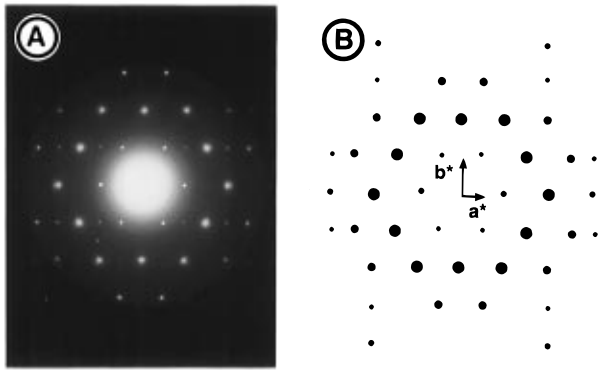


**Figure 9.** Comparison of the observed (A) and simulated (B) electron diffraction pattern for the base plane ($hk0$) of inulin monohydrate.

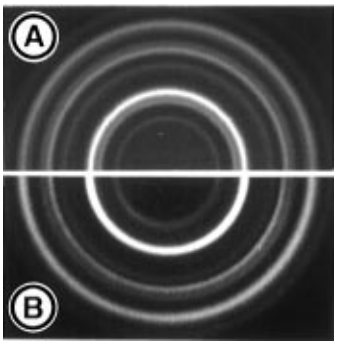


**Figure 10.** Comparison of the simulated (A) and observed (B) powder X-ray diagram of inulin monohydrate.

## Discussion

The results presented in this study confirm that inulin is a hygroscopic polysaccharide that is readily crystallizable from aqueous solutions to yield a crystal-

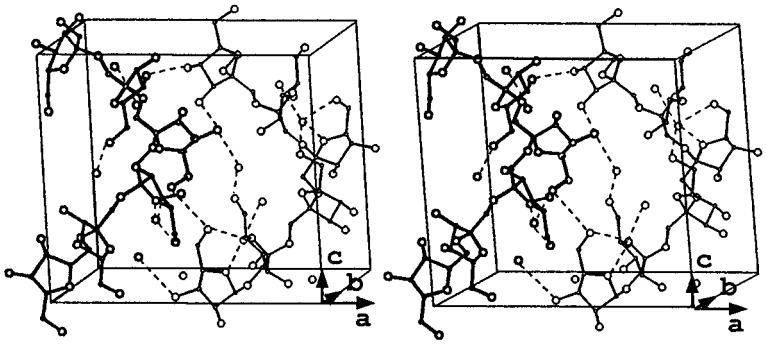


**Figure 11.** Stereoviews of the inulin monohydrate model. The dotted lines correspond to the intermolecular hydrogen bonds.

**Table 8. Summary of Conformational Parameters and Their Final Values for the Inulin Monohydrate *gt* Model**

| parameter | final value | parameter | final value |
|---|---|---|---|
| $\phi$ (deg) | 67.7 | $\tau_1$ (deg)[a] | 115.9 |
| $\psi$ (deg) | 158.6 | $\tau_2$ (deg)[a] | 109.2 |
| $\omega$ (deg) | −87.0 | $\mu$ (deg) | 21.54 |
| $\chi_o$ (deg) | 39.0 | $W$ | 0.715 |
| $\chi_c$ (deg) | 161.2 | | |

[a] Unlike the other conformational parameters, $\tau_1$ and $\tau_2$ were not varied during the refinement.

**Table 10. Summary of Intermolecular Hydrogen Bond Interactions Stabilizing the Structure of Inulin Monohydrate**

| donor atom | acceptor atom | $d$ (Å) | residues[a] |
|---|---|---|---|
| O4 | O4 | 2.57 | $I_2-II_1$ |
| O4 | O3 | 3.31 | $I_1-II_1$ |
| O6 | O6 | 3.40 | $I_1-II_6$ |
| O6 | O3 | 3.10 | $I_2-III_5$ |
| O3 | O3 | 2.55 | $II_1-III_6$ |
| O3 | O4 | 3.18 | $II_2-III_6$ |
| $O_W$ | O4 | 2.57 | $W_5(II)-I_1$ |
| $O_W$ | O6 | 2.52 | $W_2(I)-I_2$ |
| $O_W$ | O6 | 2.65 | $W_6(I)-I_1$ |
| $O_W$ | O6 | 2.54 | $W_6(I)-I_6$ |

[a] The chain II is defined as in Table 9. The chain III is generated from chain I by $(x', y', z') = (x, 1 + y, z)$. The atomic coordinates of the residues and those of the oxygens of the water molecule are defined as in Table 9 in the Supporting Information.

line monohydrate containing one molecule of water per fructosyl residue. Half of this intracrystalline water is fairly labile as it is able to leave the crystal upon air or vacuum drying. In the resulting hemihydrate, the remaining water appears to be firmly bound and almost impossible to remove without destruction of the crystals. Our observations on the hydration of well-characterized single crystals of inulin are consistent with the earlier work of Katz and Derksen,[2] who were the first to mention the two states of hydration of inulin crystals. The differences that we have observed between the diffraction diagrams of the inulin monohydrate and the hemihydrate are similar to those reported earlier but not explained, either by Katz and Derksen[2] or by Marchessault *et al.*[4] The present work goes one step further as it gives a molecular rationale for these differences.

**Structure of Inulin Hemihydrate.** In terms of molecular description, our inulin hemihydrate model, derived from the *hk*0 and *hkl* structure factor amplitudes and the LALS methodology, is devoid of any short inter- or intramolecular contacts. This model corresponds to a regular sixfold helix (right-handed) of (2→1) $\beta$-D-fructofuranose with the five-membered ring in the lowest energy conformation $^4T_3$. The relative orientation of adjacent monomer units is described by torsion angles having values of $\phi = 66°$, $\psi = 154.5°$, and $\omega = -81.8°$. Among the three conformations *tg*, *gt*, and *gg* for the hydroxymethyl group, the *gt* conformation ($\chi_o = 54.1°$, $\chi_c = 176.2°$) is preferred in terms of energy and *R* factor. The conformation with the *tg* structure ($\chi_o = 174.5°$) leads to a refinement slightly less favorable. On the other hand, the differences between the *gt* and *gg* orientation ($\chi_o = -60.9°$) are more significant.

In the case of glycosidic torsion angles $\phi$ and $\psi$, it is known both experimentally and theoretically [18] that there exists a preference for *gauche* conformers about the anomeric C−O bond. This *gauche* preference arises from the influence of the exo-anomeric effect.[19] The rotation around the aglycon C−O bond is less restricted although the lowest energy conformers usually exhibit also a *gauche* orientation with respect to the aglycon hydrogen. The values of $\phi$ and $\psi$ obtained for the best inulin hemihydrate model are consistent with these findings: the conformation about the bond C2′−O1 is indeed *gauche*; similarly, the conformation about C1−O1 is also *gauche* with respect to the two aglycon hydrogens. Regarding the $\omega$ torsion angle, this conformation differs somewhat from the exact *gauche* situation since our $\omega$ angle, refined to the value of −81.8°, is more than 20° away from the exact *gauche* canonical form. It is likely that this deviation is due to the constraint required to obtain the helical sixfold symmetry. It appears that this constraint is borne mostly by the $\omega$ angle, which must be the most flexible from the three torsion angles that define the conformation of the inulin helix.

In the Marchessault *et al.* inulin model,[4] a fivefold helix (right handed) was proposed with linkage torsion angles having values $\phi = 75°$, $\psi = 130°$, and $\omega = -60°$ (using our definition). These values differ by 9° for $\phi$, −24.5° for $\psi$, and 22° for $\omega$. These differences may be accounted for by the difference in helical symmetry: sixfold in our case as opposed to fivefold in the case of Marchessault *et al.*[4] Our diffraction data rule out the fivefold helical symmetry, which would require placing the inulin chains off the crystallography screw dyad axes. This would lead to four chains (20 fructosyl residues) per unit cell instead of two chains (12 residues) with a concomitant density increase. Alternatively, one might consider a doubling of either the *a* or *b* unit cell dimension to form a four-chain unit cell. This doubling is inconsistent with our base plane dimensions ($a = 16.70$ Å and $b = 9.65$ Å) which are firmly established by our electron diffraction patterns. In light of these observations, the fivefold conformation is therefore ruled out.

It is interesting to compare the geometry of our inulin chain with that of the inulobiosyl residues in inulobiose,[9]

kestose,[20] and nystose.[21] For instance, the conformation analysis of inulobiose using different force fields[9] has predicted a minimum energy structure with the $^4T_3$ conformation for the fructofuranose rings and a glycosidic linkage with torsion angle values of $\phi = 51.6°$, $\psi = 168.8°$, and $\omega = 57°$. These values of $\phi$ and $\psi$ are in the same region as those found for the present inulin model. An exception is the angle $\omega$, for which a significantly different orientation has been found. The crystal structures of two oligosaccharides, namely 1-kestose[22] [α-D-glucopyranoside, *O*-β-D-fructofuranosyl-(2→1)-β-D-fructofuranosyl] and nystose trihydrate[23,24] [α-D-glucopyranoside, *O*-β-D-fructofuranosyl-(2→1)-*O*-β-D-fructofuranosyl-(2→1)-β-D-fructofuranosyl trihydrate], that contain an inulobiose moiety have been reported. The observed values of the glycosidic torsion angles are $\phi = 80.5°$, $\psi = -169.7°$, and $\omega = 179.2$ for 1-kestose. Nystose contains two inulobiosyl units and independent studies[23,24] agreed that their $\phi$, $\psi$, and $\omega$ values are (171.2°, −133.3°, −63.3°) and (71.6°, −165.1°, −175.9°), respectively. The $\phi$ and $\psi$ values in the crystal conformation of the inulobiose moiety exhibit similarities with those found here for inulin. In both cases, the molecules are linked by an extensive system of hydrogen bonds.[22−24] However, in these oligosaccharide structures, all hydroxyl groups are involved in intermolecular hydrogen bonds and there is no intramolecular hydrogen bonding as in our inulin model.

In three-dimensional polysaccharide structures, hydrogen bonding generally involves all hydroxyl groups as both donors and acceptors. Hydrogen bonds are usually identified by the O···O distances in the range of 2.5−3.4 Å. Using this criterion, a survey of the O···O distances in the proposed hemihydrate inulin structure should give two intramolecular medium hydrogen bonds between O5(I)···O6(I) and O3($I_2$)···O1($I_1$) atoms. However, the facts that (a) the donor and acceptor are separated by three bonds and (b) the angles defined by [C6−O6···O5 and C3−O3···O1] deviate from 110° by more than 30° imply that the geometry of these two "hydrogen bond" interactions is far from linear and merely a consequence of minimizing torsional and nonbonded energy in the three-bond system. Table 5 indicates that there are six intermolecular hydrogen bonds between the inulin chain indicated by short O···O distances and six intermolecular hydrogen bonds involving water molecules and inulin chains. Among the six intermolecular hydrogen bonds, three of them, namely O3($I_2$)···O3($II_1$), O6($I_1$)···O6($II_6$), and O6($I_1$)···O4($III_5$), correspond to O···O distances that are larger than 3.1 Å and, therefore, these interactions can be referred to as weak. In our model, the O4($I_2$)···O4($II_1$) and O6($I_2$)···O3($III_5$) interactions are medium ($d_{O\cdots O}$ = 2.7−2.8 Å). A strong interaction between O3($II_1$)···O3($III_6$) at $d_{O\cdots O} = 2.52$ Å is also observed. In addition to the short O···O distances, we have also found a short distance between the C4−H4 group of the residue $II_1$ and the oxygen atom O3 of the residue $I_2$. These short H4(II1)···O3($I_2$) and C4($II_1$)···O3($I_2$) distances of 2.13 and 3.14 Å, respectively, suggest the presence of attractive interactions known as C−H···O hydrogen bonds.[25] The six intermolecular hydrogen bonds between water molecules and polysaccharide chains can be referred to as medium interactions since the oxygen to oxygen distances are between 2.7 and 3.3 Å. The proposed network of intermolecular hydrogen bonds in inulin is illustrated in Figure 8.

The simulation of the electron diffractograms, achieved here with the CERIUS software, is another way to illustrate the reliability of our model of crystalline inulin. In the case of inulin hemihydrate, there is almost a perfect correspondence between the observed *hk*0 diffractogram and the calculated one (Figure 5). One exception, however, is the 040 spot (marked with an arrow in Figure 5A), which is observed as a medium-intensity spot but is not shown in the calculated diagram (Figure 5B). The difference in observed and calculated *F* values for the reflection 040 is also shown in Table 2 which, on the other hand, indicates that a fairly good fit exists for all the other 47 *hkl* reflections. At present, we do not have any explanation for the occurrence of a weak 040. We assume that a better fit between the observed and calculated data and in particular the 040 diffraction spot could result from relaxing the fructosyl ring geometry. A second possibility would be to investigate the result of setting models with fructosyl conformations other than $^4T_3$. A third option would allow for different ring conformations and linkages for three successive fructosyl residues, since the asymmetric unit is actually the trisaccharide. However, none of these approaches was followed here as each would introduce a large number of additional parameters which are not justified by the number of experimental diffraction data. The quality of the existing fit between observed and calculated data indicates that the use of such flexible models would not have a large effect on either the general shape or the interactions of the polymer.

The simulation of the oriented and unoriented X-ray diffraction diagrams of inulin hemihydrate is quasi perfect (Figure 6). All the features of the diffraction diagram of inulin hemihydrate reported here, or the earlier studies of Katz and Derksen[2] as well as Marchessault *et al.*,[4] are readily apparent in the simulated diagrams in Figures 6A and 6C. Remarkably, the strong diffraction line at $d = 8.32$ Å (marked with an arrow in Figure 6B and 6D) that is present only in the hemihydrate and totally absent in the X-ray diagram of the hydrate is well represented, both in position and in intensity in the simulated diagrams. It is interesting to notice that the simulated X-ray diagrams presented here were obtained for an inulin hemihydrate model derived from electron diffraction data only. With these data, no Lorentz and polarization correction was applied for the intensities and the corresponding *F* values were taken directly as the square root of the diffraction intensities. This lack of correction which could be questioned otherwise appears therefore justified, at least in light of the visual comparison of the observed and calculated X-ray diagrams.

**Structure of Inulin Monohydrate.** The structure of inulin monohydrate, derived from the electron diffraction *hk*0 data set, is very similar to the structure of the hemihydrate, with the exception of the number of water molecules that are present in the unit cell. As for the case of the hemihydrate, the monohydrate structure consists also of a regular right-handed sixfold helix. The mutual orientation of the monomer units is described by torsion angles having values of $\phi = 67.7°$, $\psi = 158.6°$, and $\omega = -87.0°$. The hydroxymethyl groups are oriented in the same *gt* conformation with $\chi_o = 39.0°$ and $\chi_c = 161.2$ °. A comparison of these values with those of the hemihydrate allomorph indicates that the conformation of the inulin chain remains nearly the same in going from the hemihydrate to the monohy-

drate. In fact, the slight conformational variations, borne essentially by the $\psi$ and $\omega$ angles, must correspond to the slight increase of 0.3 Å in the *c* (helix) axis repeat distance.

As in the case of the hemihydrate, the intraresidue O6···O5 and O3···O1 contacts are suggestive of hydrogen bonds but we do not consider them as such for the reasons noted in our discussion of that structure. The crystals of inulin monohydrate are stabilized by a series of intermolecular hydrogen bonds. These are listed in Table 10 and illustrated in Figure 11. Six intermolecular hydrogen bonds are found. Two of them are fairly strong as they correspond to O···O distances lower than 2.6 Å, whereas the four others are much weaker, with distances above 3 Å. Among the six water molecules of the structure, four of them are connected to the inulin chains whereas the two remaining are associated together in a cluster. With the exception of W4, all the other water molecules are hydrogen bonded by fairly strong bonds ($O_W \cdots O_W \sim 2.5-2.6$ Å).

A survey of the list of hydrogen bonds of the structure of inulin monohydrate indicates that this structure appears to have a cohesion that is much stronger than that of the hemihydrate, where the molecules of water are held by rather weak bonds. Furthermore, in the hemihydrate, the occupancy of the water molecules was only 0.75 as opposed to 1 in the case of the monohydrate. When comparing the details of the hydrogen bonds in the inulin hemihydrate (Table 5) and monohydrate (Table 10), one sees that the hydroxymethyl oxygens O6 of the inulin chains are all engaged in hydrogen bonds that are stronger with inulin monohydrate. This difference is quite significant and we believe it could well account for the rather large decrease of 15° that is found for the angle $\chi_o$ when the inulin hemihydrate is further hydrated to give the monohydrate structure. A final interesting feature observed in Table 10 is that one water molecule W4 participates in one C−H···$O_W$ hydrogen bond (H1b(II3)···$O_W$(W4(II)) of 2.1 Å). This pattern of hydration fits into the survey of Steiner and Saenger [26] that describes the general case of C−H···O in the coordination of water molecules.

As expected from the low *R* factor achieved for the inulin monohydrate, the simulated *hk*0 electron diffraction pattern is quite consistent with the observed diffractogram (Figure 9). However, unlike the inulin hemihydrate case, where the agreement between the observed and simulated X-ray diffractograms was excellent, this agreement is less perfect in the monohydrate structure (Figure 10). For example, the reflection at $d = 8.32$ Å is totally absent in the observed X-ray pattern but calculated as a weak one in the simulated pattern that is deduced from the electron diffraction data refinement. The reason for this difference must be due to the slight differences in hydration arising from the different techniques used for keeping the sample under hydrated conditions. The frozen hydrated method employed in electron diffraction involved quench cooling of the hydrated crystals to liquid nitrogen temperature while in the X-ray case the crystals were equilibrated at 95% relative humidity and then sealed in capillary tubes for examination at room temperature. Thus the inulin monohydrate structure which was refined with the electron diffraction data does not correspond exactly to the state of hydration in the samples used for the X-ray experiments.

The occurrence of the weak composite diffraction spot 110 and 200 at $d = 8.32$ Å in the electron diffraction patterns of inulin monohydrate and the absence of this diffraction maximum in the corresponding X-ray patterns reflects the lability of some of the water molecules in this polymorph. Previously, it has been noted both by Katz and Derksen[2] and by Marchessault *et al.*[4] that the disappearance of this composite reflection could be directly correlated with the full hydration of inulin monohydrate. Our results seem to confirm these observations, and the occurrence of weak 110 and 200 electron diffraction spots indicates that a full hydration was not maintained during the electron diffraction experiments, despite the use of the frozen hydrated method. This technique should in principle preserve all the water of crystallization within the hydrated crystalline lattice, but does not seem to do so in the present case. This observation is consistent with a scheme of hydration for the crystals of inulin monohydrate where there would be two types of water molecules within the lattice. Half of them—those of the hemihydrate structure—are so tightly bound that they will remain even after a harsh annealing treatment.[2,4] The other half appears to be fairly labile and quite difficult to maintain completely within the crystalline lattice. The diffraction line at 8.32 Å is thus a very sensitive probe to monitor the amount of this labile water.

The hydration results presented in this study were obtained with inulin that was extracted from chicory and then recrystallized. As inulin constitutes a substantial percentage of the total root mass of chicory, it would be interesting to see whether similar hydration/dehydration results could be obtained on the root tissues themselves. One of the established functions of inulin in specific plants is that of a carbohydrate reserve.[1] It remains to be seen whether the hydration pattern encountered in inulin has any specific ecological and biological significance.

**Acknowledgment.** I.T. was a recipient of a two year CNRS fellowship. W.T.W. had a three month visiting professorship from the Joseph Fourier University of Grenoble.

**Supporting Information Available:** $F_o(hkl)$ and $F_c(hkl)$ values for the inulin hemihydrate (Table 2) and inulin monohydrate (Table 7) *gt* models and fractional coordinates for three independent residues of the asymmetric unit of one chain of inulin hemihydrate (Table 4) and inulin monohydrate (Table 9) (8 pages). This material is contained in many libraries on microfiche, immediately follows this article in the microfilm version of the journal, can be ordered from the ACS, and can be downloaded from the Internet; see any current masthead page for ordering information and Internet access instructions.

## References and Notes

(1) Hendry, G. *New Phytol.* **1987**, *106* (*Suppl.*), 201.
(2) Katz, J. R.; Derksen, J. C. *Recl. Trav. Chim. Pays-Bas* **1931**, *50*, 247.
(3) Katz, J. R.; Weidinger, A. *Recl. Trav. Chim. Pays-Bas* **1931**, *50*, 1133.
(4) Marchessault, R. H.; Bleha, T.; Deslandes, Y.; Revol, J. F. *Can. J. Chem.* **1980**, *58*, 2415.
(5) André, I.; Putaux, J. L.; Chanzy, H.; Taravel, F. R.; Timmermans, J. W.; de Wit, D. *Int. J. Biol. Macromol.* **1996**, *18*, 195.
(6) IUPAC−IUB Joint Commission on Biochemical Nomenclature. *Eur. J. Biochem.* **1983**, *131*, 5.
(7) Sundaralingan, M. *Biopolymers* **1968**, *6*, 189.
(8) Chanzy, H.; Guizard, C.; Vuong, R. *J. Microsc.* **1977**, *111*, 143.
(9) Calub, T. M.; Waterhouse, A. L.; French, A. D. *Carbohydr. Res.* **1990**, *207*, 221.
(10) Boutherin, B. CERMAV, personal communication.
(11) Smith, P. J. C.; Arnott, S. *Acta Crystallogr., Sect. A* **1978**, *A34*, 3.

(12) Chanzy, H.; Pérez, S.; Miller, D.; Paradossi, G.; Winter, W. T. *Macromolecules* **1987**, *20*, 2407.
(13) *International Tables for X-ray Crystallography*; Kynoch Press: Birmingham, England, 1968; Vol. III.
(14) Arnott, S.; Winter, W. T. *Fed. Proc., Fed. Am. Soc. Exp. Biol.* **1977**, *36*, 73.
(15) The crystallographic residuals $R$ and $R$" are calculated as follows: $R = \sum(||kF_o| - |F_c||)/\sum|kF_o|$; $R'' = \{\sum[w(|kF_o| - |F_c|)^2]/\sum w(kF_o)^2\}^{1/2}$, where $k$ is the scale factor and $w$ is the weight given to individual reflections. In this work, $w = 1$ was taken for the $F(hk0)$ and $w = 0.5$ and 0.1 were used for $F(hkl)$ corresponding to the observed and unobserved reflections, respectively.
(16) CERIUS 2 and QUANTA, Molecular Simulations, Burlington, MA.
(17) French, A. D.; Tran, V. *Biopolymers* **1990**, *29*, 1599.
(18) Tvaroska, I.; Bleha, T. *Adv. Carbohydr. Chem. Biochem.* **1989**, *47*, 45.
(19) Lemieux, R. U.; Pavia, A. A.; Martin, J. C.; Watanabe, K. A. *Can. J. Chem.* **1969**, *47*, 4427.
(20) Waterhouse, A. L.; Calub, T. M.; French, A. D. *Carbohydr. Res.* **1991**, *217*, 29.
(21) French, A. D.; Mouhous-Riou, N.; Pérez S. *Carbohydr. Res.* **1993**, *247*, 51.
(22) Jeffrey, G. A.; Park, Y. J. *Acta Crystallogr.* **1972**, *B28*, 257.
(23) Okuyama, K.; Noguchi, K.; Saitoh, M.; Ohno, S.; Fujii, S.; Tsukada, M.; Takeda, H.; Hidano, T. *Bull. Chem. Soc. Jpn.* **1993**, *66*, 374.
(24) Jeffrey, G. A.; Huang, D. *Carbohydr. Res.* **1993**, *247*, 37.
(25) Sutor, D. J. *J. Chem. Soc.* **1963**, 1105.
(26) Steiner, T.; Saenger, W. *J. Am. Chem. Soc.* **1993**, *115*, 4540.

MA951799F